Journal of Polymers and the Environment (2023) 31:501–518
https://doi.org/10.1007/s10924-022-02614-y

ORIGINAL PAPER

A pH-Sensitive Surface of Chitosan/Sepiolite Clay/Algae Biocomposite for the Removal of Malachite Green and Remazol Brilliant Blue R Dyes: Optimization and Adsorption Mechanism Study

Zahirah Mohd Zain[1] · Ahmed Saud Abdulhameed[2,3] · Ali H. Jawad[1] · Zeid A. ALOthman[4] · Zaher Mundher Yaseen[5,6,7]

Accepted: 26 September 2022 / Published online: 1 November 2022

Abstract

A pH-sensitive chitosan/sepiolite clay/algae biocomposite (Chi/Sep/Alg) was fabricated to remove cationic (malachite green, MG) and anionic (remazol brilliant blue R, RBBR) dyes from aqueous. The characteristics of Chi/Sep/Alg biocomposite were investigated by pH_{pzc}, pH-potentiometric titration, CHNS, XRD, SEM–EDX, FTIR, and BET analyses. A Box–Behnken design (BBD) was adopted to optimize the adsorptive performance of the Chi/Sep/Alg biocomposite towards removal of MG and RBBR dyes using three controllable operating factors, namely Chi/Sep/Alg dose (0.02–0.1 g), solution pH (4–8), and process time (5–30 min). The ideal BBD model circumstances for MG dye removal efficiency were as follows: Chi/Sep/Alg dose (0.1 g/L), solution pH 8, and time (17.5 min), while for RBBR dye, the ideal circumstances were Chi/Sep/Alg dose (0.1 g/L), pH ~ 4, and time (17.5 min). The adsorption kinetic and isotherm reflect that the adsorption of MG and RBBR dyes onto Chi/Sep/Alg biocomposite obeyed pseudo-second-order and Freundlich isotherm model, respectively. The maximum adsorption capacities of Chi/Sep/Alg biocomposite towards MG (515.7 mg/g) at basic pH environment (pH 8) and RBBR (292.4 mg/g) at acidic pH environment (pH 4). An endothermic and spontaneous adsorption process of MG and RBBR dyes was confirmed by the calculated thermodynamic functions. The adsorption mechanism of MG and RBBR dyes on the surface of Chi/Sep/Alg biocomposite can be attributed to various interactions such as electrostatic, H-bonding, and n-π interactions. Thus, this pH-sensitive Chi/Sep/Alg biocomposite exhibits a great affinity towards capturing cationic and anionic dyes by adjusting the solution pH.

Keywords Adsorption · Algae · Anionic and cationic dyes · Chitosan · Sepiolite clay · Optimization

Introduction

The discharge of hazardous environmental pollutants i.e., heavy metals, pharmaceuticals, pesticides, and organic dyes from industrial sectors like plastics, cosmetics, paper, textiles, antiseptics, leather, and food to aquatic environments have significantly damaged their characteristics [1]. Organic dyes are one of the typical environmental pollutants, which have a significant threat to aquatic life and human beings due to their carcinogenicity, high toxicity, and non-biodegradability, where a tiny quantity of dyes discharged into freshwater has an impact on aquatic life and food webs [2–4].

✉ Ali H. Jawad
ali288@uitm.edu.my; ahjm72@gmail.com

1 Faculty of Applied Sciences, Universiti Teknologi MARA, 40450 Shah Alam, Selangor, Malaysia

2 Department of Medical Instrumentation Engineering, Al-Mansour University College, Baghdad, Iraq

3 College of Engineering, University of Warith Al-Anbiyaa, Karbala, Iraq

4 Chemistry Department, College of Science, King Saud University, Riyadh 11451, Saudi Arabia

5 Department of Earth Sciences and Environment, Faculty of Science and Technology, Universiti Kebangsaan Malaysia, 43600 Bangi, Selangor, Malaysia

6 Adjunct Research Fellow, USQ's Advanced Data Analytics Research Group, School of Mathematics Physics and Computing, University of Southern Queensland, Darling Heights, QLD 4350, Australia

7 New Era and Development in Civil Engineering Research Group, Scientific Research Center, Al-Ayen University, Thi-Qar 64001, Iraq

The persistence of dyes' aromatic structure is likely to be responsible for the mutagenic and carcinogenic issues in nature [5]. Based on these serious consequences resulting from the increased pollution of water with organic dyes, it is necessary to treat wastewater before it is released into the freshwater. Generally, several methods such as coagulation/flocculation [6], adsorption [7–9], membrane filtration [10], photocatalytic degradation [11], and oxidation [12] were extensively carried out for the removal of organic dyes from contaminated wastewaters. However, most of these methods have some drawbacks, for example, high energy requirements, generation of high amounts of sludge, and formation of toxic byproducts [13]. Among these aforementioned methods, adsorption is listed as one of the most successful and widely used methods for treating organic dyes is due to its efficiency, ease of application, environmental friendliness, strong controllability, low cost, and high selectivity [14].

Chitosan (Chi) is a linear polysaccharide synthesized from partial deacetylation of chitin and it is predominantly composed of the unbranched chains of D-glucosamine units [15, 16]. Chi has a set of unique properties e.g., abundance in nature, biodegradability, adsorption ability, nontoxicity, antimicrobial activity, hydrophilicity, biocompatibility, and high chemical reactivity [17]. The presence of the active sites (amino and hydroxyl groups) in the Chi matrix makes it a desirable adsorbent for the removal of anionic dyes through the electrostatic interactions between protonated amino groups ($–NH_3^+$) of the Chi and the anionic groups of the dyes in solid/liquid interface solution [18]. However, there is a weakness of Chi when used as an adsorbent in adsorption technologies like pH-dependent (soluble or gel form at acidic medium), low mechanical/thermal performance, and low surface area [19]. From this standpoint, several ways e.g., composition, crosslinking, and grafting have been presented to modify various properties of Chi [20]. The design of Chi-based composites has been extensively introduced as a unique approach for modifying characteristics of Chi such as adsorption ability, swelling/water adsorption, mechanical performance, and surface area [21]. Several outstanding biological and natural materials e.g., montmorillonite (MMT) mineral [22], algae (Alg) biomass [23], and sepiolite (Sep) clay [24] have been employed to form Chi composites due to their promising chemical and physical characteristics, as well as their naturally abundant, sustainable, and environmentally friendly properties.

Sep clay is one of the abundant and widely used inorganic minerals as an effective adsorbent for the removal of organic/inorganic pollutants from water due to its remarkable properties such as high porosity, high specific surface area, adsorption of cationic pollutants, mechanical stability, environmentally friendly, and low cost [25]. Sep is characterized by its fibrous structure with the formula of $Mg_8(H_2O)_4Si_{12}O_{30}(OH)_4{\cdot}8H_2O$ [26]. This property leads to the penetration of many organic and inorganic pollutants into the structure of Sep [27]. Thus, formulation of Chi biopolymer with Sep clay leads to present an ideal absorbent to absorb both anionic and cationic contaminants as well as overcoming some of Chi's weaknesses [28, 29].

In the same context, the use of biomaterials as effective, sustainable, and inexpensive biosorbents (e.g., algae, agricultural waste, and bacteria) for the removal of different contaminants from wastewater has gained great attention [30, 31]. Algae (Alg) is one of the interesting biomaterials used as biosorbent for water decontamination due to its renewable, inexpensive, available year-round, high adsorption affinity, and relatively high surface area [32]. Alg is characterized by the presence of reactive functional groups in its structure such as hydroxyl (–OH), carboxyl (–COOH), phosphate ($–PO_4^{-3}$), and amino ($–NH_2$) groups, which can bind with different inorganic/organic pollutants through electrostatic attraction, complexation, and ion exchange [33]. Recently, several studies have shown that unmodified Alg and Alg composite have a high adsorption capacity for the removal of metal ions and organic dyes from polluted water [34, 35].

Thus, the present study aims to prepare a new pH-sensitive chitosan/sepiolite clay/algae biocomposite (Chi/Sep/Alg) with unique surface property and capability towards removing both cationic (malachite green, MG) and anionic (remazol brilliant blue R, RBBR) dyes from aqueous environment. A variety of instrumental approaches including zero point of charge (pH_{pzc}), CHNS Analyzer, Brunauer Emmet Teller (BET), X-ray diffraction (XRD), Fourier transform infrared (FTIR) spectra, scanning electron microscopy (SEM), and pH-potentiometric titration were employed to investigate the physicochemical properties of Chi/Sep/Alg biocomposite. A statistical approach of response surface methodology (RSM) with Box-Behnken design (BBD) was applied to explore the operational factors (Chi/Sep/Alg dose, pH, and time) affecting the responses including MG dye removal (%) and RBBR dye removal (%). Kinetic and adsorption isotherm study of MG and RBBR dyes was performed. A realistic adsorption mechanism for MG and RBBR dye molecules on the surface of Chi/Sep/Alg biocomposite was proposed.

Materials and Methods

Materials

Chitosan (Chi) biopolymer (deacetylation ≥ 75%), and sepiolite clay (Sep) powder were ordered from Sigma–Aldrich, while algae (Alg) was laboratory synthesized. The dyes used in adsorption experiments including malachite green (MG) as a model of cationic dye with

molecular weight ($C_{23}H_{25}ClN_2$; MW: 364.911; g/mol $\lambda_{max} = 617$ nm), and remazol brilliant blue R, (RBBR) as a model of anionic dye ($C_{22}H_{16}N_2Na_2O_{11}S_3$; MW: 626.54; g/mol $\lambda_{max} = 592$ nm) were provided from R&M Chemicals, Malaysia. The mother chemical reagents (e.g., sodium chloride powder, hydrochloric acid, sodium hydroxide pellets, and acetic acid) were supplied from R&M Chemicals, Malaysia. Deionized water was utilized to prepare all the dyes stock solution and other required solutions throughout this study.

Synthesis of Chi/Sep/Alg

Chi/Sep/Alg biocomposite was prepared by adding 100 mL of 5% acetic acid solution to a mixture of Chi flakes (2 g), Alg powder (1 g), and Sep clay powder (1 g). Then, the viscous solution was vigorously stirred by a magnetic stirrer for 24 h to complete the dissolution of Chi flakes and achieve the composition between the three materials (Chi, Sep, and Alg). The next step included converting the viscous solution formed into Chi/Sep/Alg beads through injection of the viscous solution by a 10 mL syringe into 1000 mL NaOH (0.5 M) solution at a rate of 1 mL/min (manually). The fresh Chi/Sep/Alg beads were gently washed with distilled water several times to ensure that the traces of NaOH solution were removed. After that, the fresh Chi/Sep/Alg beads were dried in the oven for 24 h, meanwhile, Chi/Sep/Alg beads were strongly pulverized by a mortar and pestle. Lastly, the final powder of Chi/Sep/Alg biocomposite was sieved to a constant particle size of 150 < particle size > 250 µm. The structure of Chi/Sep/Alg biocomposite is proposed in Fig. 1.

Characterization

The surface physical property (e.g., specific surface area and pore volume) of the materials, namely, Sep, Alg, and Chi/Sep/Alg biocomposite were obtained using the Brunauer Emmet Teller (BET) analysis (Micromeritics ASAP 2060). The surface morphologies of Chi/Sep/Alg biocomposite and Chi/Sep/Alg biocomposite before and after adsorption of MG and RBBR dyes were inspected by a scanning electron microscope (SEM, Zeiss Supra 40 VP), meanwhile, estimation of the elemental composition for the Chi/Sep/Alg biocomposite and Chi/Sep/Alg biocomposite after MG and RBBR dyes adsorption was achieved by energy dispersive X-ray analysis (EDX). X-ray diffraction (XRD) patterns of Chi, Sep, Alg, and Chi/Sep/Alg biocomposite were obtained by a PANalytical X'Pert PRO diffractometer over the 2-theta (2θ) range from 5° to 90°. Determination of the percentage of free amino groups in the Chi/Sep/Alg biocomposite was carried out through the pH-potentiometric titration way [36]. The percentages of C, H, N, and S elements in Sep, Alg, and Chi/Sep/Alg biocomposite were determined by CHNS

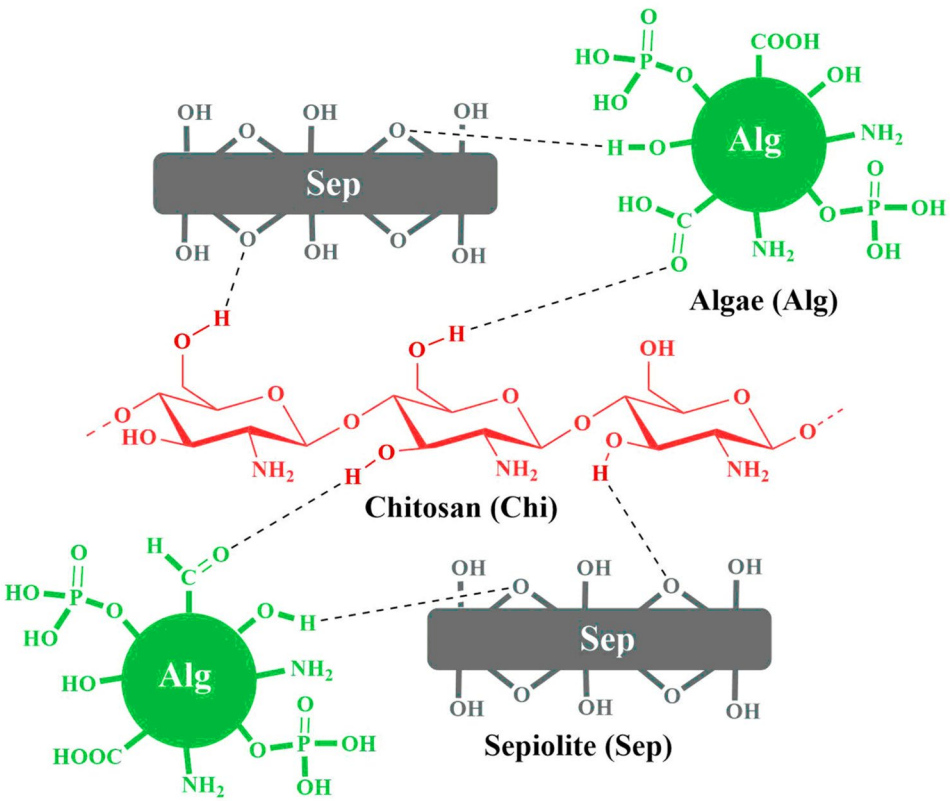

Fig. 1 Diagram demonstrating the chemical interactions between the components of the Chi/Sep/Alg biocomposite

Table 1 Codes and actual variables and their levels in BBD

Codes	Variables	Level 1 (-1)	Level 2 (0)	Level 3 (+1)
A	Chi/Sep/Alg dose (g)	0.02	0.06	0.1
B	pH	4	6	8
C	Time (min)	5	17.5	30

Analyzer (Flash 2000, Thermo-scientific). Determination of the charge on the Chi/Sep/Alg biocomposite surface was accomplished by a zero point of charge (pH_{pzc}) method [37]. Fourier transform infrared (FTIR) spectra of the Chi/Sep/Alg biocomposite and Chi/Sep/Alg biocomposite having adsorbed the MG and RBBR dyes were obtained by a Perkin-Elmer, Spectrum RX I using KBr pellets at wavenumber range from 4000 to 450 cm^{-1}.

Statistical Optimization Methodology

Herein, the optimization and study of the three key parameters i.e., Chi/Sep/Alg dose, solution pH, and process time, which have the greatest effect on the MG and RBBR dyes removal efficiency were carried out by RSM-BBD. The software known as Design Expert 13.0 (Stat-Ease, Minneapolis, USA) was utilized to design adsorption experiments and analyze the results statistically. The levels of the investigated factors and their symbols are given in Table 1. Hence, a second-order quadratic equation was utilized to infer the relationship between chosen input factors and MG and RBBR dyes removal efficiency. Equation 1 shows the mathematical formula of the polynomial statistical model.

$$Y = \beta_0 + \sum \beta_i X_i + \sum \beta_{ii} X_i^2 + \sum \sum \beta_{ij} X_i X_j \quad (1)$$

Y is the expected response (MG and RBBR dyes adsorption efficiency (%)), while X_i and X_j belong to the independent adsorption variables. β_0 β_i, β_{ii}, and β_{ij} are the regression constants for the intercept, linear, square effect, and interaction effect, respectively. Accordingly, seventeen runs were derived from BBD to evaluate and optimize the influence of the three variables i.e., Chi/Sep/Alg dose (A: 0.02–0.1 g), pH (B: 4–10), and time (C: 5–30 min) on the percentage removal of MG and RBBR dyes. Table 2 summarizes the ranges of the investigated parameters as well as the corresponding observed responses (MG dye removal (%) and RBBR dye removal (%)). Experimentally, the first step involved adding a specified mass of Chi/Sep/Alg biocomposite to a set of 250 ml Erlenmeyer flasks containing 100 ml of the MG or RBBR dye solution. Then, these samples were taken to a water bath shaker (WNB7-45, Memmert, Germany) to stir gently (100 strokes/min) at a specified time. Afterward, the samples were filtered by a syringe

Table 2 The 3-variables BBD matrix and experimental data for MG removal and RBBR removal

Run	A: Dose (g)	B: pH	C: Time (min)	MG removal (%)	RBBR removal (%)
1	0.02	4	17.5	14.7	70.1
2	0.1	4	17.5	30.5	95.7
3	0.02	8	17.5	26.3	65.8
4	0.1	8	17.5	78.5	72.9
5	0.02	6	5	16.3	53.8
6	0.1	6	5	31.1	70.8
7	0.02	6	30	30.2	75.1
8	0.1	6	30	74.1	79.2
9	0.06	4	5	10.6	78.9
10	0.06	8	5	20.3	51.4
11	0.06	4	30	29.1	86.6
12	0.06	8	30	61.6	92.9
13	0.06	6	17.5	44.7	84.7
14	0.06	6	17.5	47.6	88.9
15	0.06	6	17.5	50.8	89.7
16	0.06	6	17.5	44.9	83.5
17	0.06	6	17.5	48.5	88.1

filter (0.45 µm) to obtain the adsorbent-free dye solutions. The residual concentration in MG and RBBR solutions was spectrophotometrically (UV–Vis, HACH DR 2800) measured at λ_{max} 617 nm and 592 nm for MG and RBBR dyes, respectively. The removal efficiency (R %) of MG and RBBR dyes was estimated by the following formulas (2):

$$R\% = \frac{(C_o - C_e)}{C_o} \times 100 \quad (2)$$

where C_o and C_e symbolize the initial and equilibrium concentrations of MG and RBBR dyes (mg/L), respectively.

Adsorption Study of MG and RBBR Dyes on Chi/Sep/Alg

The determination of the amount of dye adsorbed onto the Chi/Sep/Alg biocomposite was achieved through batch adsorption experiments. The results presented in Table 2 declare that experiments 4 and 2 gave the best percentage removal for MG (78.5%) and RBBR (95.7%) dyes, respectively. The conditions of experiment 4 related to the highest MG dye removal (%) were Chi/Sep/Alg dose (0.1 g/L), pH ~ 8, and time (17.5 min), while the conditions of experiment 2 related to the highest RBBR dye removal (%) were Chi/Sep/Alg dose (0.1 g/L), solution pH 4, and time (17.5 min). Additionally, the data indicated that Chi/Sep/Alg has the property of Zwitterion due to the results presented

Table 3 The physicochemical properties of the Sep, Alg, and Chi/Sep/Alg

Analysis	Sep	Alg	Chi/Sep/Alg
C (wt. %)	0.081	45.49	31.40
H (wt. %)	1.36	6.54	5.25
N (wt. %)	0	9.60	5.54
S (wt. %)	0	0.20	0
$–NH_2$ content (%)	–	–	31.48
BET surface area (m^2/g)	333.2	0.830	10.16
Langmuir surface area (m^2/g)	430.2	1.753	15.12
Total volume in pores (cm^3/g)	0.644	0.002	0.047
Mean pore diameter (nm)	7.71	10.89	18.53

in Table 2, especially the experiment No. 8, where a considerable removal of the MG (74.1%) and RBBR (79.2%) was recorded at pH 6, which indicates that the Chi/Sep/Alg carried negative and positive charges at pH 6, which enabled it to adsorb cationic and anionic dyes. The adsorption runs were performed at these optimal conditions with taking into account different initial concentrations of MG and RBBR dyes (20–250 mg/L) and contact time (0–360 min). Batch adsorption experiments for MG and RBBR dyes were carried out by following the same steps mentioned in the aforementioned Sect. (2.4). The mass of dye adsorbed onto the Chi/Sep/Alg biocomposite at equilibrium (q_e) was estimated by the following formulas (3):

$$q_e = \frac{(C_o - C_e)V}{W} \tag{3}$$

where V is the volume of dye solution (L) and W is the mass of Chi/Sep/Alg adsorbent (g).

Results and Discussion

Characterization of Chi/Sep/Alg

A set of physical and chemical properties of Chi/Sep/Alg biocomposite are shown in Table 3. pH-potentiometric titration is a fundamental analysis to determine the percentage of free amino groups ($–NH_2$) present in Chi/Sep/Alg biocomposite's structure, which represents active adsorption sites for acidic dyes such as RBBR dye [15, 19]. The result of the potentiometric titration revealed that the percentage of $–NH_2$ in the Chi/Sep/Alg biocomposite was 31.48%. This result indicates that the Chi/Sep/Alg contains sufficient $–NH_2$ to adsorb RBBR dye molecules. Estimation of the elemental content for Sep clay mineral, Alg, and Chi/Sep/Alg biocomposite was obtained by CHNS analysis. The CHNS results of Sep, Alg, and Chi/Sep/Alg biocomposite are given in Table 3. The CHNS data showed that the C and N contents of Chi/Sep/Alg biocomposite reduced proportionally with the increase of Sep clay mineral in the Chi/Alg matrix, indicating the Sep was successfully intercalated in the Chi/Alg matrix.

Regarding the results of BET analysis, they were as follows: Sep = 333.2746 m^2/g, Alg = 0.8306 m^2/g, and Chi/Sep/Alg biocomposite = 10.1659 m^2/g. Indeed, the surface area of Chi/Sep/Alg biocomposite is approximately higher than most of the Chi/clay and Chi/biomass composites reported in the literature, for example, magnetic kaolin/Chi beads (2.12 m^2/g) [38], Chi/vermiculite biocomposite (7.91 m^2/g) [39], and magnetic Chi/marine macro-algae biochar (6.17 m^2/g) [40]. This result corresponds to the fact that Sep clay has a prodigious surface area of 333.27 m^2/g, which acts on enlarging the surface area of the Chi/Sep/Alg biocomposite by scattering of Sep particles on the Chi/Alg biocomposite matrix. In the same context, BET's results also revealed that Chi/Sep/Alg is a mesoporous biomaterial due to its average pore diameter of 18.53 nm. This characteristic causes that the process of uptaking the MG and RBBR dye molecules into the pores of the Chi/Sep/Alg biocomposite takes place easily.

The XRD analysis was applied to get information on the crystalline bio/natural materials (Chi, Alg, and Sep) present in Chi/Sep/Alg's structure as well as to describe the crystallinity of the prepared biocomposite (Chi/Sep/Alg). The XRD patterns of Chi biopolymer, Alg biomass, Sep clay, and Chi/Sep/Alg biocomposite are given in Fig. 2. In Fig. 2a, the feature diffraction peaks at $2\theta \cong 10°$ and $2\theta \cong 20°$ are related to the crystalline regions established by hydrogen bonds between the hydroxyl (–OH) and amino ($–NH_2$) groups of the Chi chains [41]. It can be seen from the XRD pattern of Alg (Fig. 2b) that there is a characteristic peak at $2\theta = 22.5°$, which is associated with the crystalline structure of cellulose, while the peak is located at 18.5° is related to the amorphous regions of Alg biomass [42]. In Fig. 2c, the apparent peaks at $2\theta = 7.1°$, 11.8°, 13.1°, 19.7°, 20.7°, 28.2°, 29.5°, 34.6°, and 39.5° indicate that the characteristic reflections of the Sep clay, which correspond to those contained in Sep JCPDS Card (No. 75–1597([43]. The XRD pattern of Chi/Sep/Alg biocomposite (Fig. 2d) was similar to the XRD pattern of Sep with a slight change in the intensity of some peaks. This observation can be reasonably attributed to the intercalation of Alg and Chi into the interlayer region of Sep, causing the formation of the Chi/Sep/Alg biocomposite.

FTIR analysis was used to reveal one of the distinguishing characteristics of Chi/Sep/Alg biocomposite, which is knowing the type of effective groups present on Chi/Sep/Alg's surface, and thus estimating the ability of Chi/Sep/Alg biocomposite to adsorb ionic and cationic pollutants. Figure 3 appears FTIR spectra of **a** Chi/Sep/Alg biocomposite before adsorption and Chi/Sep/Alg biocomposite

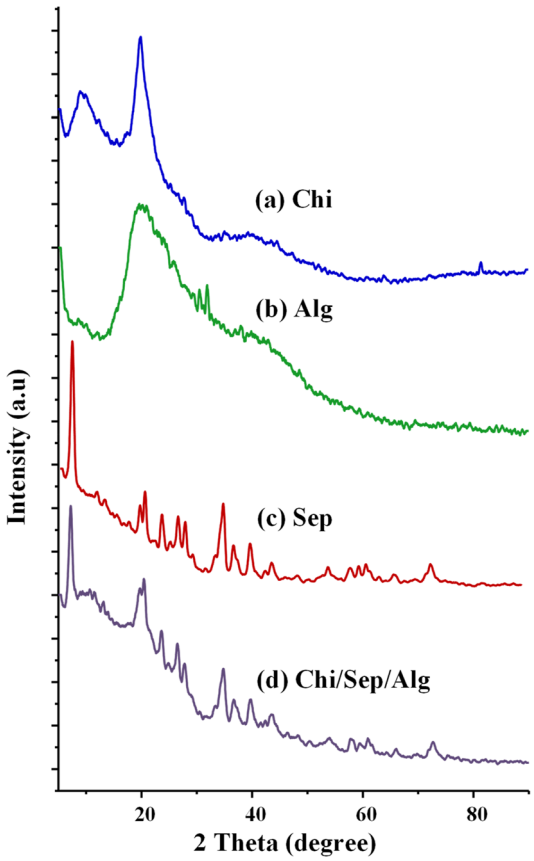

Fig. 2 XRD patterns of **a** Chi biopolymer, **b** Alg biomass, **c** Sep clay, and **d** Chi/Sep/Alg biocomposite

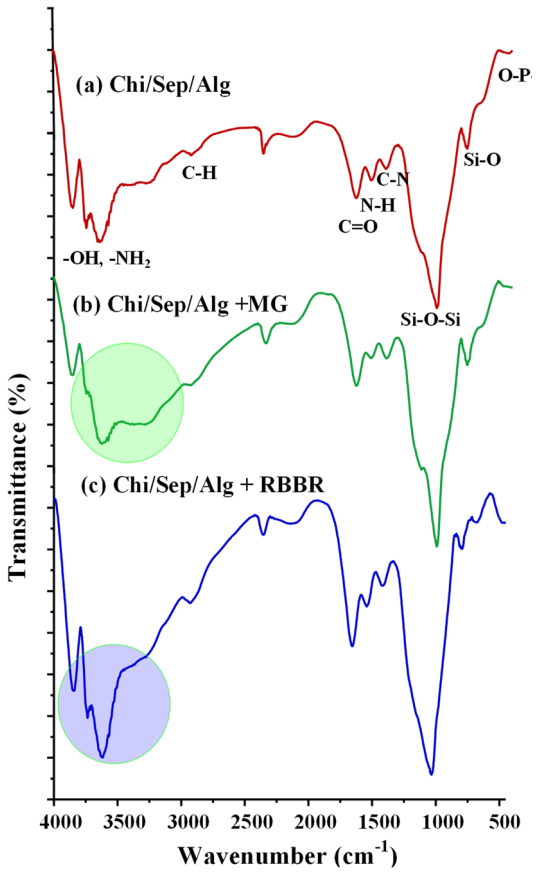

Fig. 3 FTIR spectra of **a** Chi/Sep/Alg biocomposite, and Chi/Sep/Alg biocomposite after adsorption of **b** MG and **c** RBBR dyes

after adsorption of (b) MG and **c** RBBR dyes. The FTIR spectrum of Chi/Sep/Alg biocomposite showed that the characteristic peaks at 3370–3740 cm^{-1} correspond to combining stretching vibrations of hydroxyl (–OH) and amino ($–NH_2$) groups [24, 32]. The peak located at 2926 cm^{-1} is correlated with C-H symmetric and asymmetric stretching vibrations in -CH and $-CH_2$ [24]. The peaks (Fig. 3a) at 1650 cm^{-1}, 1520 cm^{-1}, 1325 cm^{-1}, 1070 cm^{-1}, 874 cm^{-1}, and 545 cm^{-1} are assigned to stretching vibration of C = O, bending vibration of N–H, stretching vibration of C-N, symmetrical stretching vibration of Si–O-Si, bending vibration of Si–O, and vibration of O–P–O bond, respectively [27, 34]. The FTIR spectra of the Chi/Sep/Alg biocomposite after adsorption of MG (Fig. 3b) and RBBR (Fig. 3c) dyes show to have a broadly similar spectrum to the Chi/Sep/Alg biocomposite with slight shifts in some bands specifically –OH, $–NH_2$, signifying that the major functional groups of the Chi/Sep/Alg biocomposite were involved in the MG and RBBR dyes adsorption.

The morphological structure and chemical composition of the Chi/Sep/Alg biocomposite prior to and after the adsorption of the MG and RBBR dye molecules were studied by SEM–EDX analysis. Figure 4 appears the SEM images and EDX spectra of (a) Chi/Sep/Alg biocomposite before adsorption and Chi/Sep/Alg biocomposite after adsorption of (b) MG and (c) RBBR dyes. As per Fig. 4a, the morphological structure of Chi/Sep/Alg biocomposite seems obviously as a cragged and cracked surface with the presence of many crevices and small visible cavities that are randomly distributed. EDX analysis revealed that the prime elements in the Chi/Sep/Alg biocomposite are carbon, oxygen, nitrogen, silicon, and magnesium. The presence of Si and Mg elements denotes the successful composition of Sep clay within the ternary formula Chi/Sep/Alg. After adsorption of MG (Fig. 4b) and RBBR (Fig. 4c) dyes, the morphological structures of Chi/Sep/Alg biocomposite were clearly changed to be more compact with the obvious diminishing of porosity and cracks, signifying uptake of MG and RBBR dyes on the surface of the Chi/Sep/Alg biocomposite. The presence of carbon, oxygen, nitrogen, silicon, and magnesium elements in Chi/Sep/Alg biocomposite after MG dye adsorption was confirmed by EDX analysis. Regarding the EDX analysis

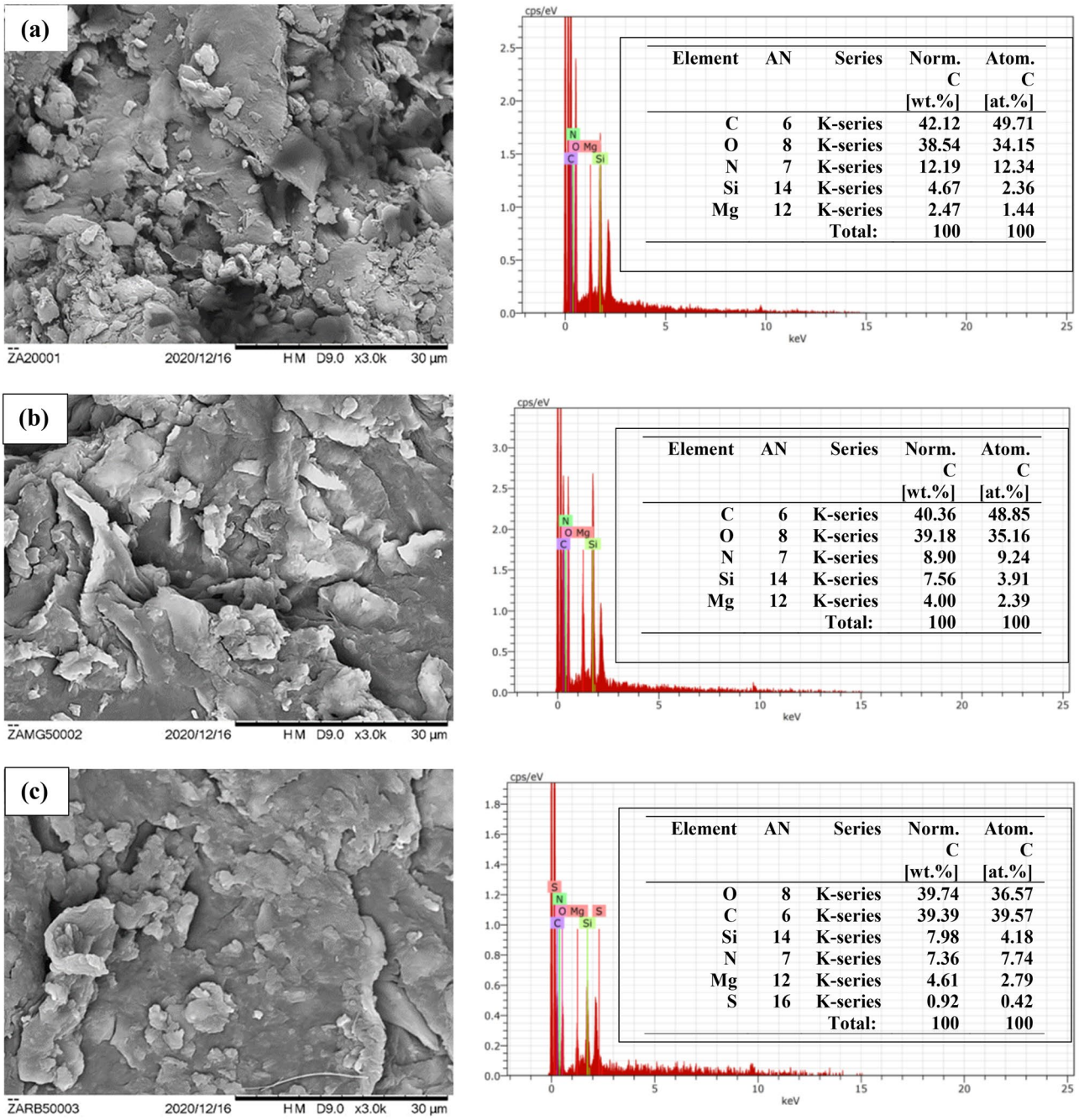

Fig. 4 SEM images and EDX spectra of **a** Chi/Sep/Alg biocomposite, and Chi/Sep/Alg biocomposite after adsorption of **b** MG and **c** RBBR dyes

of the Chi/Sep/Alg biocomposite after the adsorption of RBBR dye, the analysis revealed the presence of sulfur, which undoubtedly indicates the adsorption of RBBR dye on the surface of the Chi/Sep/Alg biocomposite, where sulfur is one of the elements in the formula of RBBR dye.

BBD Model Analysis

Analysis of variance (ANOVA) is a fundamental tool in examining the acceptability of the applied models (MG dye removal and RBBR dye removal) and analyzing the significance and adequacy of the MG and RBBR dyes removal data. The ANOVA outcomes for MG and RBBR

Table 4 Analysis of variance (ANOVA) for MG removal and RBBR removal

MG dye removal						RBBR dye removal				
Source	Sum of Squares	df	Mean Square	F-value	p-value	Sum of Squares	df	Mean Square	F-value	p-value
Model	6330.59	9	703.40	64.78	< 0.0001	2536.46	9	281.83	20.06	0.0003
A-Dose	2006.61	1	2006.61	184.80	< 0.0001	361.81	1	361.81	25.75	0.0014
B-pH	1295.40	1	1295.40	119.30	< 0.0001	291.61	1	291.61	20.76	0.0026
C-Time	1702.36	1	1702.36	156.78	< 0.0001	778.15	1	778.15	55.38	0.0001
AB	331.24	1	331.24	30.51	0.0009	85.56	1	85.56	6.09	0.0430
AC	211.70	1	211.70	19.50	0.0031	41.60	1	41.60	2.96	0.1290
BC	129.96	1	129.96	11.97	0.0106	285.61	1	285.61	20.33	0.0028
A^2	5.45	1	5.45	0.5017	0.5016	363.39	1	363.39	25.86	0.0014
B^2	315.95	1	315.95	29.10	0.0010	10.31	1	10.31	0.7340	0.4200
C^2	285.71	1	285.71	26.31	0.0014	267.12	1	267.12	19.01	0.0033
Residual	76.01	7	10.86			98.35	7	14.05		
Lack of Fit	49.71	3	16.57	2.52	0.1966	68.70	3	22.90	3.09	0.1522
Pure Error	26.30	4	6.57			29.65	4	7.41		
Cor Total	6406.60	16				2634.81	16			

dyes removal are given in Table 4. The results presented in Table 4 specifically F-values signify that the adequate of the applied models including MG dye removal and RBBR dye removal, where F- values of MG and RBBR dyes removal are 64.78 (p-value < 0.0001) and 20.06 (p-value = 0.0003), respectively. The determination coefficients (R^2) for MG and RBBR dyes removal are 0.98 and 0.96, respectively. These results indicate that the experimented and calculated data are in great agreement with each other [44]. Generally, terms having a p-value of more than 0.05 are considered to be nonsignificant on the MG and RBBR dyes removal efficiency and vice versa. For this reason, the terms of the MG dye removal model including A, B, C, AB, AC, BC, B^2, and C^2 were determined to be statistically significant, while the significant terms of the RBBR dye removal model were A, B, C, AB, BC, A^2, and C^2. Thus, the second-order quadratic polynomial models involving the responses (MG dye removal and RBBR dye removal) and tested factors after correlation were achieved as shown in Eq. 4 and Eq. 5.

$$\text{MG removal}(\%) = +47.30 + 15.84A + 12.72B + 14.59C + 9.10AB + 7.28AC + 5.70BC - 8.66B^2 - 8.24C^2 \quad (4)$$

$$\text{RBBR removal}(\%) = +86.98 + 6.73A - 6.04B + 9.86C - 4.63AB + 8.45BC - 9.29A^2 - 7.96C^2 \quad (5)$$

In addition to the above, the model plots also contribute to validating the applied models through examining the nature of the distribution of the residuals as well as knowing the degree of agreement between the experimental and theoretical values of MG and RBBR dyes removal. The plots of the normal probability of the residuals belonging to the two models MG dye removal and BBBR dye removal are shown in Fig. 5a and Fig. 5b, respectively. In Fig. 5a and Fig. 5b, the points appear to be strongly aligned with the straight line, which indicates that the points are normally and perfectly distributed and also indicates that the residuals are independent [45]. The plots of the relationship between the experimental and theoretical values of MG and RBBR dyes removal are shown in Fig. 5c and Fig. 5d, respectively. It can be seen from Fig. 5(a, b) unambiguously that a strong correlation between the experimental responses (MG dye removal and RBBR dye removal) and those that are statistically expected, evidencing the statistical validation of the models.

Significant Interactions

Three-dimensional (3D) response surface curves were modeled to understand the influence of the studied parameters and the identification of the significant interactions between the studied parameters on the MG and RBBR dyes adsorption process. The considerable interactions between the studied parameters affecting the adsorption performance of MG and RBBR dyes, i.e. Chi/Sep/Alg biocomposite dose vs. pH (AB), and pH combined with adsorption time (BC) are shown in Fig. 6. It can be seen from the results shown in Fig. 6(a, b), which attribute to the important interaction between Chi/Sep/Alg biocomposite dose and pH that

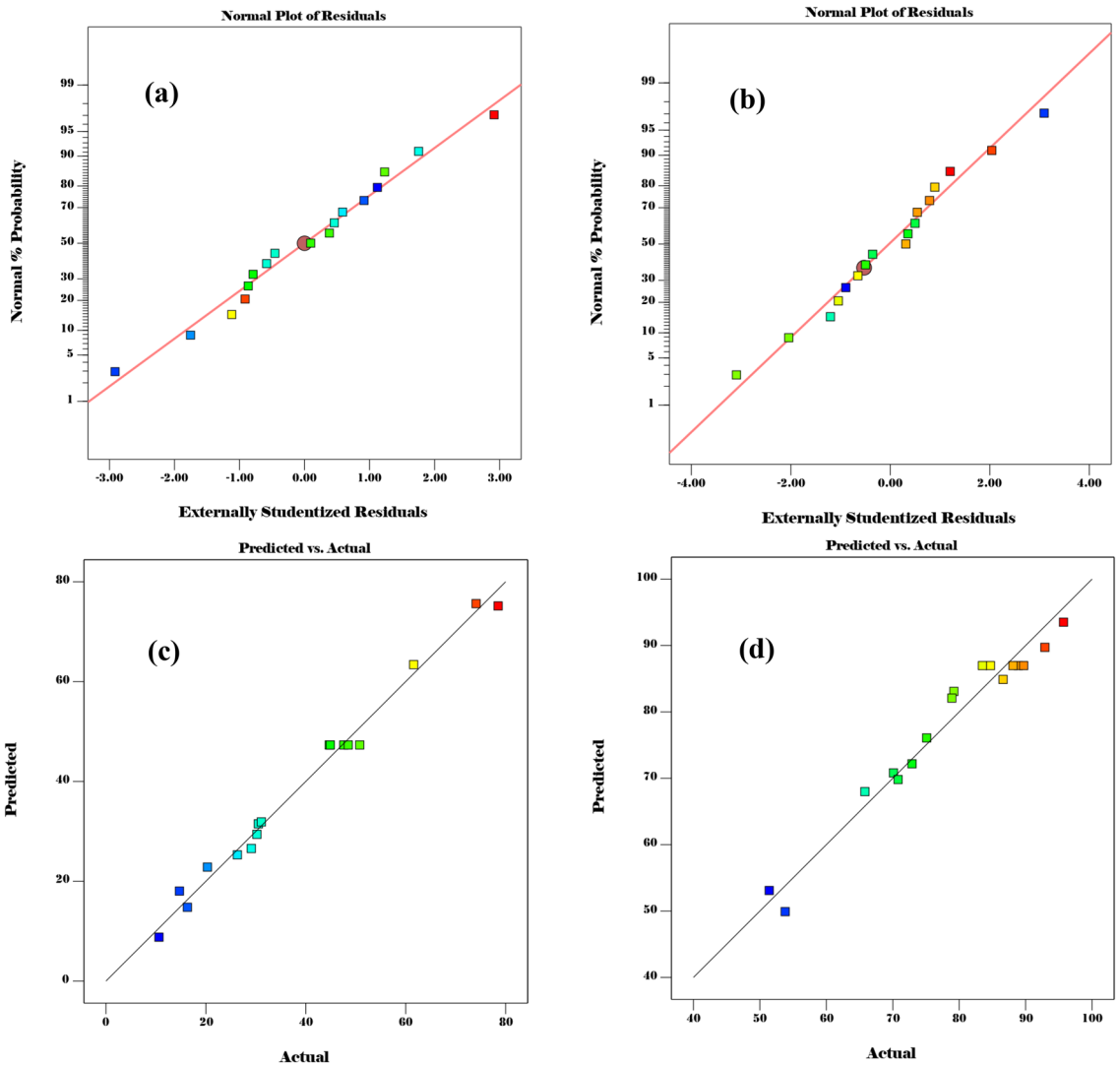

Fig. 5 Normal probability plot of residuals for **a** MG removal and **b** RBBR removal, the plot of the relationship between the predicted and actual values of **c** MG removal, and **d** RBBR removal

the sequential increase in Chi/Sep/Alg biocomposite dose from 0.02 g to 0.1 g improved the adsorption efficiency of MG and RBBR dyes. This improvement in the adsorption efficiency of MG and RBBR dyes can be attributed to the abundance of binding sites on the surface of Chi/Sep/Alg biocomposite, as well as to the surface area caused by the existence of Sep particles.

Additionally, it can be seen from the results shown in Fig. 6c, d, which attribute to the important interaction between pH and adsorption time that the sequential decrease in initial pH value from 10 to 4 improved the adsorption efficiency of RBBR, while the adsorption efficiency of MG was remarkably enhanced at basic medium (pH ~ 8). Two mechanisms can be proposed to interpret the influence of pH on MG and RBBR dyes adsorption, namely pH_{pzc} character of Chi/Sep/Alg biocomposite and the desired form (anionic or cationic) of the organic contaminant (MG or RBBR) to Chi/Sep/Alg biocomposite surface. The pH_{pzc} of Chi/Sep/Alg biocomposite was 6 as shown in Fig. 6e. As a result, at a high acidic pH level (4), i.e. less than pH_{pzc}, Chi/Sep/Alg biocomposite surface, and RBBR dye molecules are positively charged and negatively charged, respectively. On the other hand, at a high basic pH level (8), i.e. large than pH_{pzc}, Chi/Sep/Alg biocomposite surface and MG dye molecules are negatively charged and positively charged, respectively. Thus, this, in turn, enhances the affinity of Chi/Sep/Alg biocomposite towards attracting negatively/positively charged dye molecules depending on pH control, causing the improvement of MG and RBBR dyes adsorption as shown in the equations below (6) and (7), respectively.

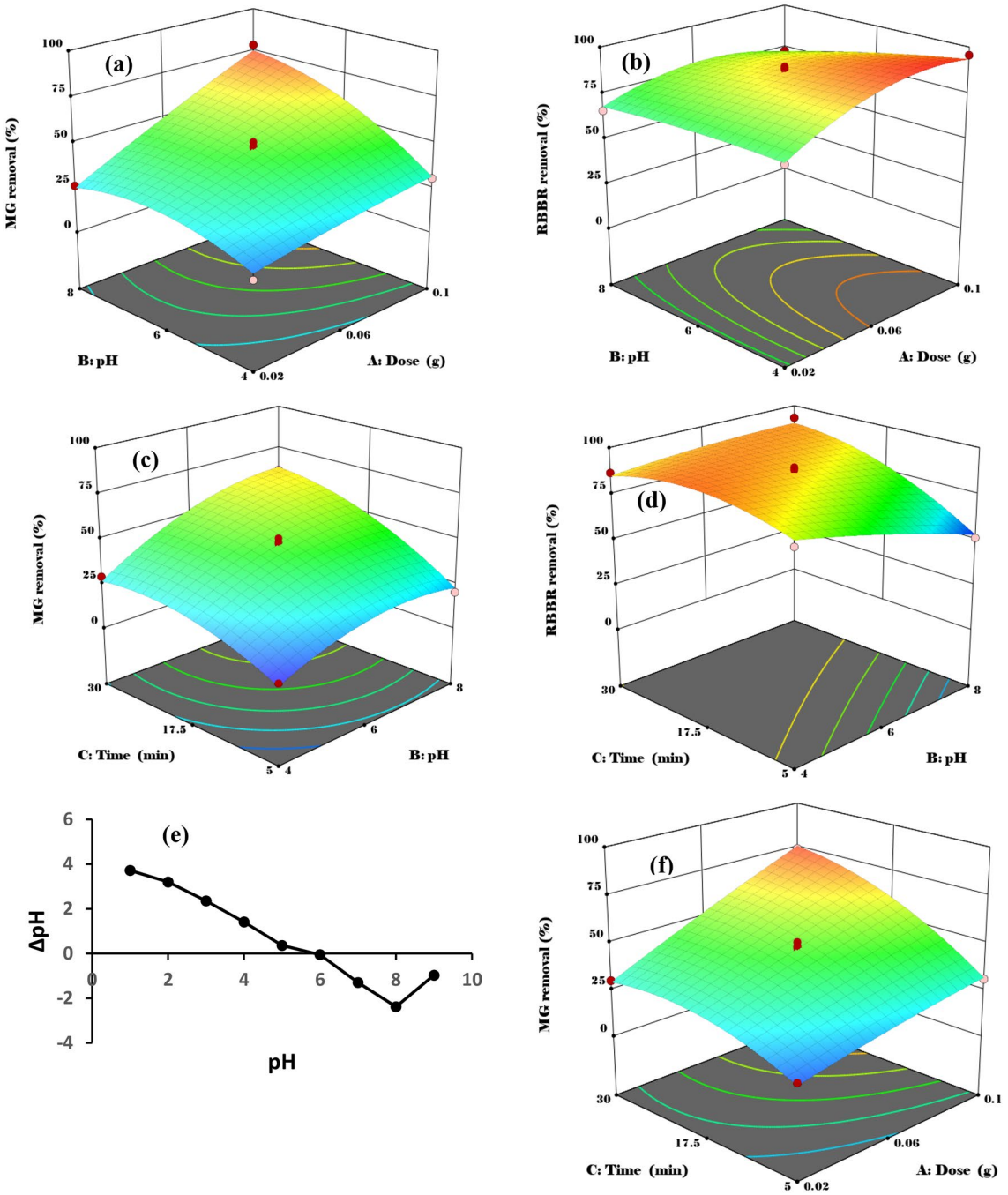

Fig. 6 3D response surfaces plots of significant interactions on MG and RBBR removal efficiency: **a** and **b** for AB interaction; **c** and **d** for BC interaction; whereas **e** pH_{pzc} of Chi/Sep/Alg and (f) AC interaction related to MG dye

$$\text{Chi/Sep/Alg}^{-} + \begin{matrix}(CH_3)\\ |\\ (MG)=N^{+}\\ |\\ (CH_3)\end{matrix} \leftrightarrow \begin{matrix}(CH_3)\,|\\ \text{Chi/Sep/Alg}^{-}\ldots{}^{+}N=(MG)\\ |\\ (CH_3)\end{matrix} \tag{6}$$

$$\begin{aligned}&\text{Chi/Sep/Alg}^{+} + (\text{RBBR}) - SO_3^{-}\\ &\leftrightarrow \text{Chi/Sep/Alg}^{+}\ldots SO_3^{-} - (\text{RBBR})\end{aligned} \tag{7}$$

The considerable interaction between Chi/Sep/Alg biocomposite dose and adsorption time (AC) affecting the adsorption performance of MG dye is shown in Fig. 6f.

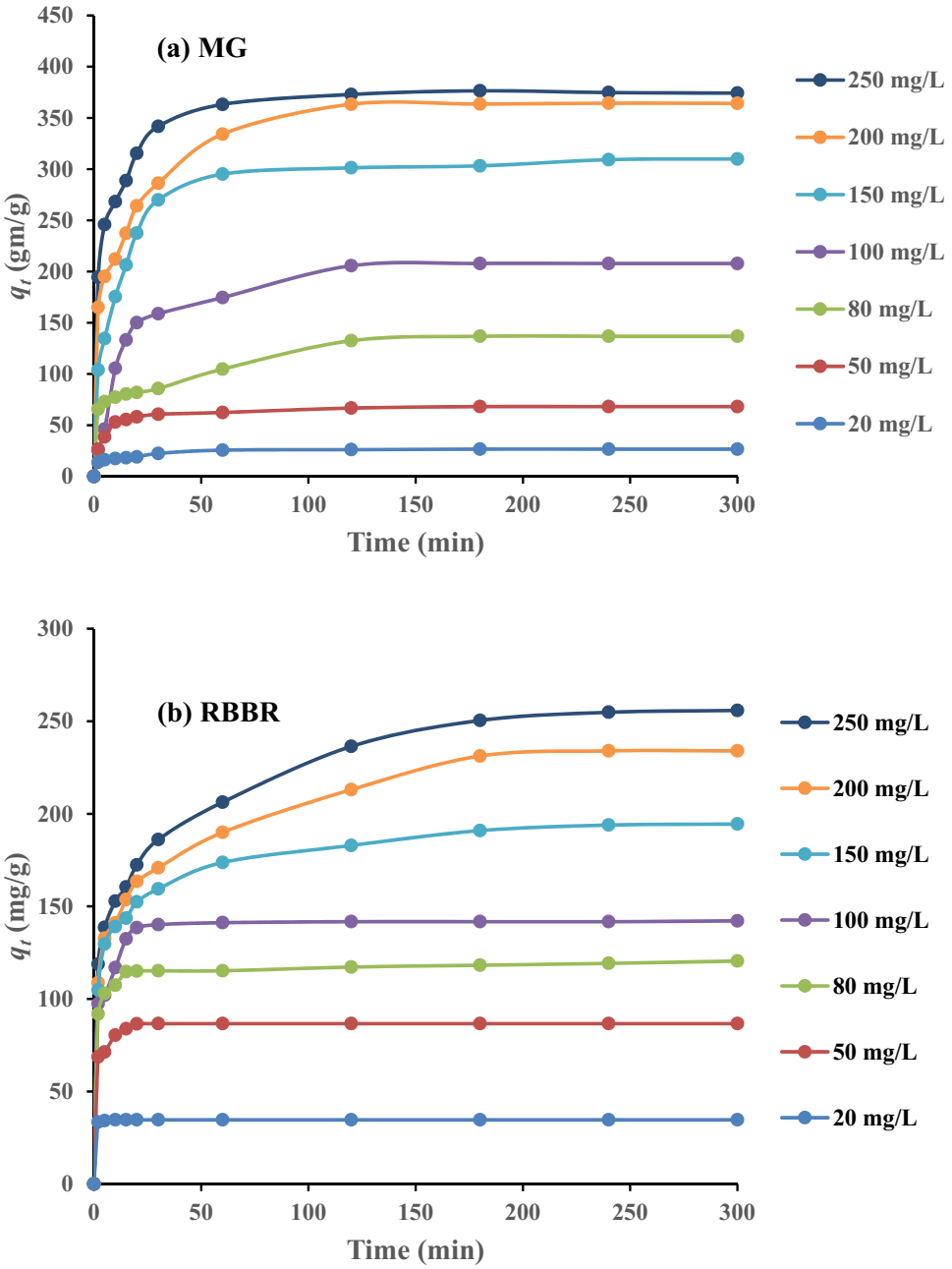

Fig. 7 **a** Effect of the contact time on adsorption of **a** MG and **b** RBBR at different initial concentrations (dose = 0.1 g, pH 8 (MG), pH 4 (RBBR), temperature = 30 °C, agitation speed = 100 strokes and volume of solution = 100 mL)

According to Fig. 6f, the adsorption performance of MG dye is significantly enhanced in line with the increase of adsorption time from 5 to 30 min, which is mostly attributed to the fact that the MG dye molecules diffuse into pores of the Chi/Sep/Alg biocomposite within a short period.

Adsorption Study

The influence of the contact time and initial MG and RBBR dyes concentration on the adsorption performance of the Chi/Sep/Alg biocomposite towards MG and RBBR dyes were explored by contacting a fixed amount of Chi/Sep/Alg biocomposite (0.1 g/100 mL) at the initial pH (8 for MG and 4 for RBBR) using a different of initial MG and RRBR concentrations (20, 50, 80, 100, 150, 200 and 250 mg/L). Figure 7(a, b) displays the curves of adsorption abilities (q_t, mg/g) of the Chi/Sep/Alg biocomposite towards the MG and RBBR dyes adsorption at initial MG and RRBR concentrations. It can be seen from Fig. 7(a, b) that there is an increasing trend of adsorption abilities of Chi/Sep/Alg biocomposite for MG and RBBR dyes with the progression of time, where adsorption ability raised from 26.6 to 374.1 mg/g for MG and from 34.7 to 255.8 mg/g for RBBR with increasing MG and RRBR dyes concentration from 20

to 250 mg/L. This is because at the higher initial dye (MG or RBBR) concentration, more dye molecules will be adsorbed on the surface of the Chi/Sep/Alg biocomposite, and as a result the adsorption capacity increases to the point that all the vacant adsorption sites on Chi/Sep/Alg biocomposite surface become occupied by dye molecules i.e., the adsorption saturation achieved [19].

Adsorption Kinetics

A kinetic model is a vital character for the comprehensive understanding of the adsorption mechanism of MG and RBBR dyes onto Chi/Sep/Alg biocomposite surface as well as identifying the rate-controlling step that is mainly responsible for MG and RBBR dyes adsorption. For this purpose, the most excessively utilized kinetic models, namely, pseudo-first-order (PFO, non-linear form as shown in Eq. 8) and pseudo-second-order (PSO, non-linear form as shown in Eq. 9) were applied to calculate kinetic parameters [46, 47].

$$q_t = q_e(1 - \exp^{-k_1 t}) \tag{8}$$

$$q_t = \frac{q_e^2 k_2 t}{1 + q_e k_2 t} \tag{9}$$

where q_t and q_e are the amount (mg/g) of adsorbed dyes and at a time (t) and in equilibrium, respectively. k_1 is the rate constant of PFO, 1/min, and k_2 is the rate constant of PSO, g/mg min. The values of the kinetic factors for the PFO and PSO models are listed in Table 5. It can be seen from the data mentioned in Table 5 that the adsorption of MG and RBBR dyes on Chi/Sep/Alg biocomposite fitted well with the PSO model. This result is related to the fact that the PSO has high values of R^2 and a close agreement between experimental ($q_{e,exp}$) and estimated ($q_{e,cal}$) values compared to the PFO model. In brief, the adsorption of MG and RBBR dyes on the Chi/Sep/Alg biocomposite is controlled by chemisorption mode i.e. chemisorption may be the phase that controls rate until equilibrium, although the whole process does not progress by a single mechanism [48].

Adsorption Isotherms

Adsorption equilibrium is a key factor to comprehensively elucidate the relationship between MG and RBBR molecules and Chi/Sep/Alg biocomposite. Consequently, the most widely utilized isotherm models including Langmuir, Freundlich, and Temkin were employed to compute the adsorption ability of the Chi/Sep/Alg biocomposite towards MG and RBBR dyes and investigate the equilibrium adsorption data [49–51]. Equations 10–12 show the non-linear forms of Langmuir, Freundlich, and Temkin, respectively.

$$q_e = \frac{q_{\max} K_a C_e}{1 + K_a C_e} \tag{10}$$

$$q_e = K_f C_e^{1/n} \tag{11}$$

$$q_e = \frac{RT}{b_T} \ln(K_T C_e) \tag{12}$$

where q_{max} is the monolayer adsorption capacity of the biocomposite and q_e is the quantity of adsorbed dyes at the solid/liquid interface. K_a (L/mg) indicates the Langmuir constant related to adsorption energy. K_f (mg/g) $(L/mg)^{1/n}$ and n are Freundlich constants. K_T (L/mg), b_T (J/mol), T (K), and R (8.314 J/mol K) signify Temkin constant, the heat of adsorption, temperature, and gas constant, respectively. Figure 8(a, b) shows the nonlinear plots (C_e versus q_e) for MG and RBBR dyes adsorption; whereas, Table 6 lists the values of isotherms parameters for MG and RBBR dyes adsorption. The resulting parameters (Table 6) denoted that the Freundlich model has a higher R^2 than the Langmuir and Temkin models, suggesting the multilayer adsorption of the MG and RBBR dyes on Chi/Sep/Alg biocomposite [52]. The kind of isotherm can be shown by values of 1/n if it is irreversible (1/n = 0), favorable (0 > 1/n < 1), or undesirable (1/n > 1). The values of 1/n in the Freundlich isotherm for MG and RBBR, respectively, were 0.50 and 0.35, indicating a desirable adsorption behavior [53]. The q_{max} values for the adsorption of MG (515.7 mg/g) and RBBR (292.4 mg/g) dyes on Chi/Sep/Alg biocomposite were compared with the other absorbents as mentioned in Table 7. Undoubtedly according to Table 7, Chi/Sep/Alg biocomposite can be effectively used as a promising bio-adsorbent in the treatment of dye-containing water.

Adsorption Thermodynamics

To explore the adsorption process of MG and RBBR dyes onto the Chi/Sep/Alg biocomposite surface in terms of spontaneity and feasibility and to determine the degree of randomness at the solid/liquid interface, adsorption thermodynamic parameters were determined. The following Eqs. (13–15) are used to calculate adsorption thermodynamic parameters such as Gibbs free energy change (ΔG°), enthalpy change (ΔH°), and entropy change (ΔS°) [55]:

$$\Delta G^\circ = -RTlnk_d \tag{13}$$

$$k_d = \frac{q_e}{C_e} \tag{14}$$

Table 5 PFO and PSO kinetic parameters for the adsorption MG and RBBR on Chi-Sep/Alg biocomposite

Concentration (mg/L)	$q_{e\ exp.}$ (mg/g)	PFO			PSO		
		$q_{e\ cal}$ (mg/g)	K_1 (1/min)	R^2	$q_{e\ cal}$ (mg/g)	$k_2 \times 10^{-2}$ (g/mg min)	R^2
MG							
20	26.6	24.2	0.191	0.82	25.9	1.155	0.93
50	68.1	64.4	0.184	0.96	68.3	0.43	0.99
80	136.8	122.2	0.095	0.71	128.8	0.134	0.84
100	207.8	201.4	0.064	0.98	220	0.038	0.98
150	309.8	299.3	0.093	0.96	317.1	0.047	0.98
200	364.2	342.3	0.109	0.85	360.2	0.054	0.94
250	374.1	349.1	0.249	0.9	370.9	0.104	0.97
RBBR							
20	34.7	34.6	1.678	0.99	34.7	37.87	0.99
50	86.6	84.6	0.745	0.97	86.9	1.78	0.99
80	120.5	115	0.747	0.98	118.1	1.348	0.99
100	142.1	136.5	0.457	0.94	142.3	0.56	0.98
150	194.4	171.1	0.337	0.87	183.2	0.246	0.96
200	233.9	203.5	0.162	0.81	218.6	0.113	0.92
250	255.8	224.9	0.134	0.8	239.6	0.092	0.91

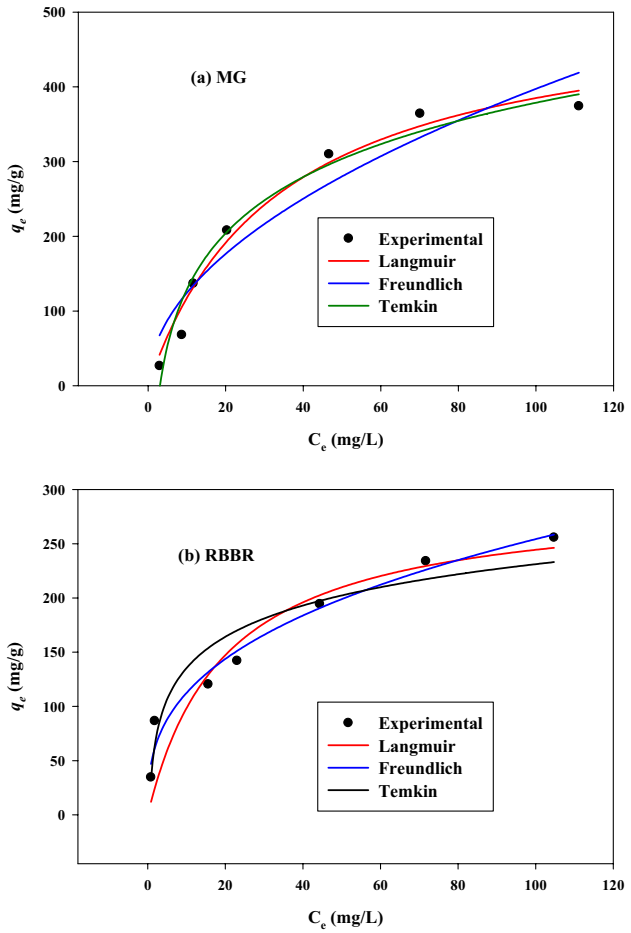

Fig. 8 Adsorption isotherms of **a** MG and **b** RBBR by Chi/Sep/Alg biocomposite (dose = 0.1 g, pH 8 (MG), pH 4 (RBBR), temperature = 30 °C, agitation speed = 100 strokes and volume of solution = 100 mL)

Table 6 Parameters of the Langmuir, Freundlich, and Temkin isotherm models for the adsorption of MG and RBBR dyes on Chi/Sep/Alg biocomposite

Adsorption isotherm	Parameter	MG	RBBR
Langmuir	q_m (mg/g)	515.7	292.4
	K_a (L/mg)	0.029	0.050
	R^2	0.98	0.87
Freundlich	K_f (mg/g) (L/mg)$^{1/n}$	38.92	49.75
	1/n	0.50	0.35
	R^2	0.92	0.97
Temkin	K_T (L/mg)	1.114	0.950
	b_T (J/mol)	23.21	60.54
	R^2	0.96	0.92

$$lnk_d = \frac{\Delta S^\circ}{R} - \frac{\Delta H^\circ}{RT} \quad (15)$$

Plotting ln k_d versus 1/T (Fig. 9) yielded the values of thermodynamic parameters (ΔH° and ΔS°), with intercept and slope representing ΔS° and ΔH°, respectively. Table 8 shows that the adsorption of MG and RBBR dyes onto the Chi/Sep/Alg biocomposite is a spontaneous and plausible process, as evidenced by the negative ΔG° values. The rising of irregularity during uptaking of MG and RBBR dyes onto the Chi/Sep/Alg biocomposite can be concluded by the positive values of $\Delta S\circ$, whilst the endothermic MG and RBBR dyes adsorption process can be inferred from positive values of ΔH° [62]. The enthalpy of MG and RBBR adsorption indicates chemisorption since the magnitude of ΔH° values for chemisorption processes is more than 20 kJ/mol [63]. Furthermore, the increase in adsorption capacity of Chi/Sep/Alg at high temperatures may be linked to the impact of temperature on the internal structure of the Chi/Sep/Alg biocomposite, which enhances the diffusion of adsorbates (MG or RBBR) in the interspaces structure of the adsorbent (Chi/Sep/Alg) [62].

Adsorption Mechanism of MG and RBBR Dyes

The adsorption mechanism of the cationic dye (MG) and the anionic dye (RBBR) was designed in light of the effective groups available on Chi/Sep/Alg's surface as shown in Fig. 10. In fact, Chi/Sep/Alg biocomposite is very abundant with active groups that can absorb both anionic and cationic pollutants, which makes it a superadsorbent called zwitterion adsorbent. These active groups come from the fact that the adsorbent is composed of natural material (Sep) and biomaterials (Chi and Alg) which in their origin are rich in active groups. Thus, the active groups are amino ($–NH_2$), phosphate (PO_4^{-3}), carboxyl (–COOH), hydroxyl (–OH), and silanol (≡Si–OH). As mentioned earlier, Chi/Sep/Alg biocomposite is a zwitterion adsorbent, and thus this enables it to adsorb MG dye in the base medium through the electrostatic attraction between the dependent group $\left(= N^+ - \left(CH_3\right)_2\right)$ of the MG dye and the negative groups (PO_4^{-3}, $–COO^-$, $–O^-$, and $\equiv Si - O^-$) of the zwitterion adsorbent (Chi/Sep/Alg). On the other hand, in the acidic medium, the Chi/Sep/Alg biocomposite acts on the adsorption of the RBBR dye through the electrostatic interactions between the sulfonate groups ($-SO_3^-$) of the RBBR dye and the positively charged groups ($-NH_3^+$,$-OH_2^+$, and $\equiv Si - OH_2^+$) of the Chi/Sep/Alg biocomposite. In addition, hydrogen interactions also play a vital role in the adsorption process for both dyes through the interaction between hydrogen on the surface of Chi/Sep/Alg's adsorbent and atoms including nitrogen and oxygen in the structure of the MG and RBBR dyes, respectively [13]. Finally, n-π's interactions contribute to the adsorption process of both dyes through the interaction between the electron-donating system represented by the nitrogen and oxygen groups in Chi/Sep/Alg's

Table 7 Comparison of the adsorption capacity of Chi/Sep/Alg biocomposite towards MG and RBBR dyes with different adsorbents

Adsorbents	Dye	q_{max} (mg/g)	References
Chi/Sep/Alg biocomposite	MG	515.7	This study
Chi/Sep/Alg biocomposite	RBBR	292.4	This study
Polymer-based bionanocomposite	MG	384.615	[54]
Magnetic NH_2-MIL-101(Al)	MG	274	[55]
Magnetic nanosized chitosan deep eutectic solvent	MG	87.72	[56]
Activated carbon (Borassus aethiopum flower)	MG	48.48	[57]
Chitosan hollow fibers	RBBR	454.5	[58]
Chitosan-glyoxal/ZnO/Fe_3O_4 nanoparticles	RBBR	363.3	[59]
ZnO-polyacrylonitrile-hinokitiol	RBBR	267.37	[60]
Paper sludge activated carbon	RBBR	158	[61]

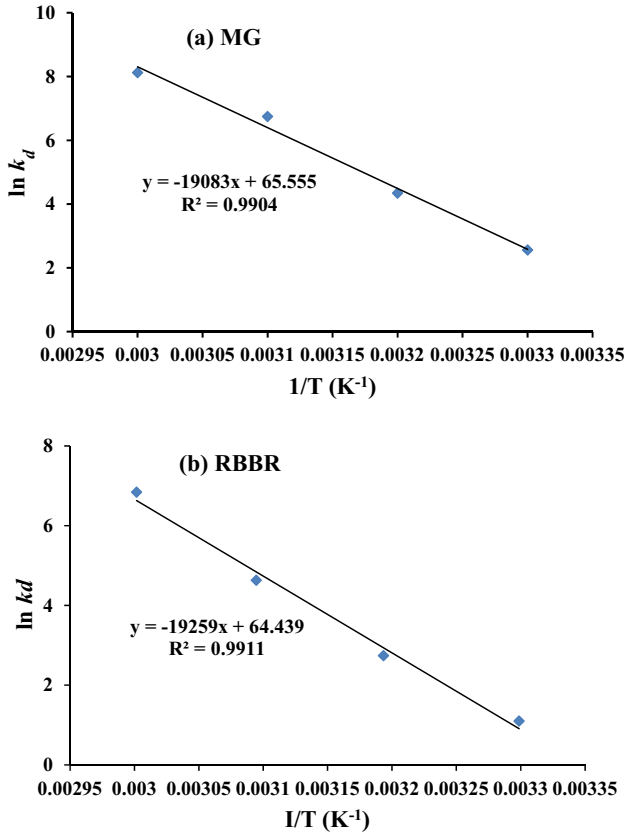

Fig. 9 Van't Hoff plot for **a** MG and **b** RBBR adsorption onto Chi/Sep/Alg biocomposite (dose = 0.1 g, pH 8 (MG), pH 4 (RBBR), agitation speed = 100 strokes and volume of solution = 100 mL)

adsorbent and the electron-gaining system represented by the aromatic rings of MG and RBBR dyes [64].

Conclusion

A new green superadsorbent of chitosan/sepiolite clay/algae biocomposite (Chi/Sep/Alg) was successfully gained by facile design and synthesis for the removal of organic dyes from aqueous solutions. The optimal conditions taken from the BBD model for MG dye removal efficiency were as follows: Chi/Sep/Alg dose (0.1 g/L), pH 8, and time (17.5 min); whereas, for RBBR dye were Chi/Sep/Alg dose (0.1 g/L), pH 4, and time (17.5 min). The highest removal of MG (78.5%) and RBBR (95.7%) dyes was obtained at these duple interactions: MG dye (AB, AC, and BC), and RBBR dye (AB, and BC). The isotherm and kinetic models confirmed that the adsorption process of MG and RBBR dye onto Chi/Sep/Alg biocomposite surface was multilayer adsorption and controlled by chemical interactions. Chi/Sep/Alg biocomposite showed remarkable absorption capacities of 515.7 mg/g and 292.4 mg/g for MG and RBBR dyes, respectively. The thermodynamic parameters stated that the adsorption process of MG and RBBR dyes was endothermic. The adsorption mechanism of MG and RBBR dyes on the surface of Chi/Sep/Alg biocomposite is carried out through chemical interactions, the most prominent of which are electrostatic, H-bonding, and n-π interactions. This work points out that Chi/Sep/Alg biocomposite could be used as a promising and effective adsorbent biomaterial for the removal of toxic dyes from wastewater.

Table 8 Thermodynamic parameters for the adsorption of MG and RBBR on Chi-Sep/Alg biocomposite

	T (K)	K_d	ΔG° (kJ/mol)	ΔH° (kJ/mol)	ΔS° (kJ/mol K)
MG	303.15	12.937	− 2.369	158.65	0.545
	313.15	209.18	− 3.823		
	323.15	850.31	− 5.128		
	333.15	3362.2	− 5.801		
RBBR	303.15	3.0035	− 0.239	160.11	0.536
	313.15	15.514	− 2.625		
	323.15	102.87	− 4.119		
	333.15	935.76	− 5.326		

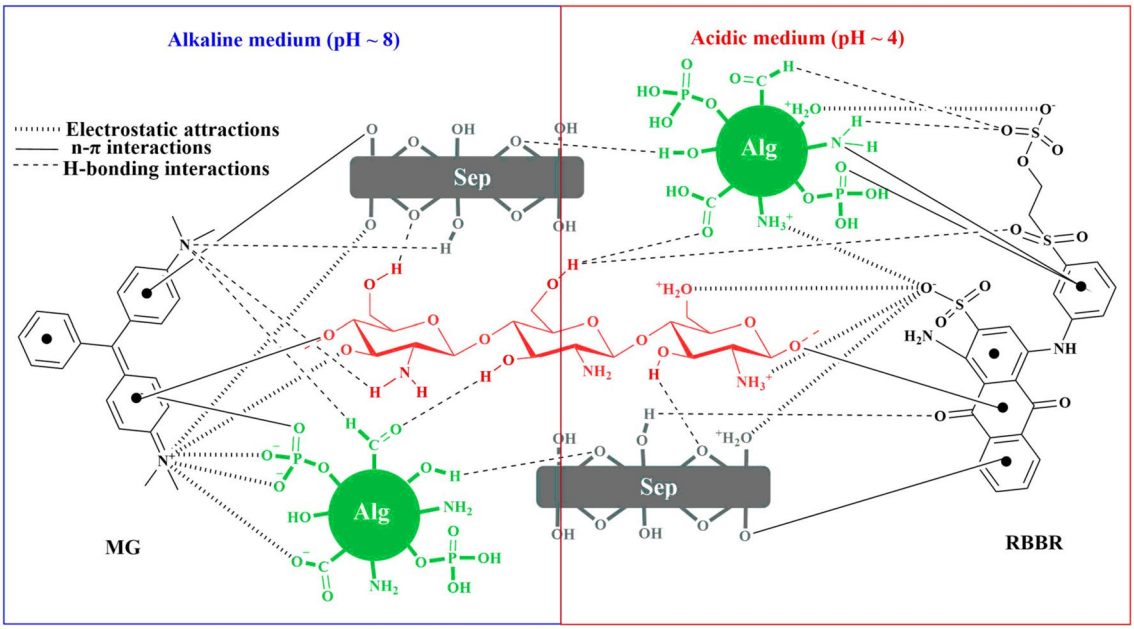

Fig. 10 Illustration of the possible interaction between Chi/Sep/Alg surface and MG and RBBR dyes including electrostatic attraction, hydrogen bonding interactions, and n-π interactions

Acknowledgements The authors would like to thank the Faculty of Applied Sciences, Universiti Teknologi MARA, Shah Alam for all facilities. The author (Zeid A. ALOthman) is grateful to the Researchers Supporting Project No. (RSP-2021/1), King Saud University, Riyadh, Saudi Arabia.

Author Contributions All authors contributed to the study conception and design. Material preparation, data collection and analysis were performed by ZMZ, ASA, AHJ, ZAA and ZMY. The first draft of the manuscript was written by ZMZ, ASA, AHJ and all authors commented on previous versions of the manuscript. All authors read and approved the final manuscript.

Funding Zeid A. ALOthman has received research support from Researchers Supporting Project No. (RSP-2021/1), King Saud University, Riyadh, Saudi Arabia.

Data Availability The datasets generated during and/or analyzed during the current study are available from the corresponding author on reasonable request.

Declarations

Competing interest The authors have no relevant financial or non-financial interests to disclose.

References

1. Jawad AH, Sahu UK, Jani NA, Z.A. ALOthman, L.D. Wilson, (2022) Magnetic crosslinked chitosan-tripolyphosphate/MgO/Fe_3O_4 nanocomposite for reactive blue 19 dye removal: Optimization using desirability function approach. Surf Interfaces 28:101698
2. Abd Malek NN, Yousif E, Jawad EAH (2020) Optimization of adsorption parameters for reactive red 4 (RR4) removal by cross-linked chitosan-epichlorohydrin using box behnken design. Sci Lett 14(1):83–95
3. Bensalah J, Berradi M, Habsaoui A, Dagdag O, El Amri A, El Khattabi O, Lebkiri A, Rifi EH (2021) Adsorption of the Orange Methyl Dye and Lead (II) by the Cationic Resin Amberlite® IRC-50: Kinetic Study and Modeling of Experimental Data. J. Chem. Soc. Pakistan. 43:5
4. Bensalah J, Berradi M, Habsaoui A, Allaoui M, Essebaai H, El Khattabi O, Lebkiri A, Rifi EH (2021) Kinetic and thermodynamic study of the adsorption of cationic dyes by the cationic artificial resin Amberlite® IRC50. Mater. Today: Proc. 45:7468–7472
5. M.P. da Rosa, A.V. Igansi, S.F. Lütke, T.R.S.A.C. Junior, A.C.R. do Santos, A.P.D.O.L. Inacio, L.A.D.A. Pinto, P.H. Beck, A new approach to convert rice husk waste in a quick and efficient adsorbent to remove cationic dye from water. J. Environ. Chem. Eng. 7(6) (2019) 103504.
6. Nnaji PC, Anadebe CV, Ezemagu IG, Onukwuli OD (2022) Potential of Luffa Cylindrica Seed as Coagulation-Flocculation (CF) Agent for the Treatment of Dye Wastewater: Kinetic, Mass Transfer, Optimization and CF Adsorption Studies. Arab J Chem 15:103629
7. Jawad AH, Kadhum AM, Ngoh YS (2018) Applicability of dragon fruit (Hylocereus polyrhizus) peels as low-cost biosorbent for adsorption of methylene blue from aqueous solution: kinetics, equilibrium and thermodynamics studies. Desalin Water Treat 109:231–240
8. Bensalah J, Benhiba F, Habsaoui A, Ouass A, Zarrouk A, Lebkiri A, El Khattabi O, Rifi EH (2022) The adsorption mechanism of the anionic and cationic dyes of the cationic resin A® IRC-50, kinetic study and theoretical investigation using DFT. J Indian Chem Soc 99(7):100512

9. El Amri A, Bensalah J, Idrissi A, Lamya K, Ouass A, Bouzakraoui S, Zarrouk A, Rifi EH, Lebkiri A (2022) Adsorption of a cationic dye (Methylene bleu) by Typha Latifolia: equilibrium, kinetic, thermodynamic and DFT calculations. Chem Data Collect 38:100834
10. Zhao J, Liu H, Xue P, Tian S, Sun S, Lv X (2021) Highly-efficient PVDF adsorptive membrane filtration based on chitosan@CNTs-COOH simultaneous removal of anionic and cationic dyes. Carbohydr Polym 274:118664
11. Rafaie HAG, Yusop NFM, Azmi NF, Abdullah NS, Ramli NIT (2021) Photocatalytic degradation of methylene blue dye solution using different amount of ZnO as a photocatalyst. Sci Lett 15(1):1–12
12. Shin J, Bae S, Chon K (2021) Fenton oxidation of synthetic food dyes by Fe-embedded coffee biochar catalysts prepared at different pyrolysis temperatures: A mechanism study. Chem Eng J 421:129943
13. Uddin MJ, Ampiaw RE, Lee W (2021) Adsorptive removal of dyes from wastewater using a metal-organic framework: A review. Chemosphere 284:131314
14. Yang X, Zhu W, Song Y, Zhuang H, Tang H (2021) Removal of cationic dye BR46 by biochar prepared from Chrysanthemum morifolium Ramat straw: A study on adsorption equilibrium, kinetics and isotherm. J Mol Liq 340:116617
15. Jawad AH, Rangabhashiyam S, Abdulhameed AS, Syed-Hassan SSA, ALOthman, Z. A., & Wilson, L. D. (2022) Process Optimization and Adsorptive Mechanism for Reactive Blue 19 Dye by Magnetic Crosslinked Chitosan/MgO/Fe3O4 Biocomposite. J Polym Environ 30(7):2759–2773
16. R. Gerhardt, B.S. Farias, J.M. Moura, L.S. de Almeida, A.R. da Silva, D. Dias, T.R.S.C. Jr, L.A. Pinto, Development of chitosan/Spirulina sp. blend films as biosorbents for Cr^{6+} and Pb^{2+} removal. Int. J. Boil. Macromol. 155 (2020) 142–152.
17. Khan A, Alamry KA (2021) Recent advances of emerging green chitosan-based biomaterials with potential biomedical applications: A review. Carbohydr Res 506:108368
18. Zhao X, Wang X, Lou T (2021) Preparation of fibrous chitosan/sodium alginate composite foams for the adsorption of cationic and anionic dyes. J Hazard Mater 403:124054
19. Jawad AH, Abdulhameed AS, Wilson LD, Hanafiah MAKM, Nawawi WI (2021) Fabrication of Schiff's base chitosan-glutaraldehyde/activated charcoal composite for cationic dye removal: optimization using response surface methodology. J Polym Environ 29(9):2855–2868
20. Saheed IO, Da Oh W, Suah FBM (2021) Chitosan modifications for adsorption of pollutants–A review. J Hazard Mater 408:124889
21. Jawad AH, Abdulhameed AS, Surip SN, Sabar S (2020) Adsorptive performance of carbon modified chitosan biopolymer for cationic dye removal: kinetic, isotherm, thermodynamic, and mechanism study. Int J Environ Anal Chem. https://doi.org/10.1080/03067319.2020.1807966
22. El-Kousy SM, El-Shorbagy HG, Abd El-Ghaffar MA (2020) Chitosan/montmorillonite composites for fast removal of methylene blue from aqueous solutions. Mater Chem Phys 254:123236
23. Saad EM, Elshaarawy RF, Mahmoud SA, El-Moselhy KM (2021) New Ulva lactuca Algae Based Chitosan Bio-composites for Bioremediation of Cd (II) Ions. J Bioresour Bioprod 6:223–242
24. Marrakchi F, Khanday WA, Asif M, Hameed BH (2016) Cross-linked chitosan/sepiolite composite for the adsorption of methylene blue and reactive orange 16. Int J Boil Macromol 93:1231–1239
25. Hu XE, Feng X, Fei M, Tian M, Zhang R, Zhou Y, Zeng Z (2021) Preparation of Acid Red73 adsorbed on chitosan-modified sepiolite with SiO_2 coating as a highly stable hybrid pigment. Dyes Pig 185:108938
26. Mahmoud MR, Rashad GM, Metwally E, Saad EA, Elewa AM (2017) Adsorptive removal of $^{134}Cs^{+}$, $^{60}Co^{2+}$ and $^{152+154}Eu^{3+}$ radionuclides from aqueous solutions using sepiolite: single and multi-component systems. Appl Clay Sci 141:72–80
27. Largo F, Haounati R, Akhouairi S, Ouachtak H, El Haouti R, El Guerdaoui A, Addi AA (2020) Adsorptive removal of both cationic and anionic dyes by using sepiolite clay mineral as adsorbent: Experimental and molecular dynamic simulation studies. J Mol Liq 318:114247
28. Khan MU, Al-Asbahi BA, Bibi S, Taimur S, Nawaz M, Yasin T, Ahmed AAA (2022) Investigations on amidoxime grafted sepiolite-based chitosan organic–inorganic nanohybrid composite beads towards wastewater detoxification. J King Saud Uni Sci 34:101689
29. Senol-Arslan D (2021) Isotherms, kinetics and thermodynamics of pb (ii) adsorption by crosslinked chitosan/sepiolite composite. Polym Bull. https://doi.org/10.1007/s00289-021-03688-9
30. Saravanan P, Josephraj J, Thillainayagam BP (2021) A comprehensive analysis of biosorptive removal of basic dyes by different biosorbents. Environ Nanotechnol Monit Manage 16:100560
31. Singh S, Kumar V, Datta S, Dhanjal DS, Sharma K, Samuel J, Singh J (2020) Current advancement and future prospect of biosorbents for bioremediation. Sci Total Environ 709:135895
32. Sun W, Sun W, Wang Y (2019) Biosorption of Direct Fast Scarlet 4BS from aqueous solution using the green-tide-causing marine algae Enteromorpha prolifera. Spectrochim Acta Part A 223, 117347
33. Doğar Ç, Gürses A, Açıkyıldız M, Özkan E (2010) Thermodynamics and kinetic studies of biosorption of a basic dye from aqueous solution using green algae Ulothrix sp. Colloids Surf B: Biointer 76:279–285
34. Almomani F, Bohsale RR (2021) Bio-sorption of toxic metals from industrial wastewater by algae strains Spirulina platensis and Chlorella vulgaris: Application of isotherm, kinetic models and process optimization. Sci Total Environ 755:142654
35. Sarojini G, Babu SV, Rajamohan N, Rajasimman M, Pugazhendhi A (2022) Application of a polymer-magnetic-algae based nanocomposite for the removal of methylene blue–Characterization, parametric and kinetic studies. Environ Pollut 292:118376
36. Vieira RS, Beppu MM (2006) Interaction of natural and crosslinked chitosan membranes with Hg (II) ions. Colloids Surf A Physicochem Eng Asp 279(1–3):196–207
37. Dalvand A, Nabizadeh R, Ganjali MR, Khoobi M, Nazmara S, Mahvi AH (2016) Modeling of Reactive Blue 19 azo dye removal from colored textile wastewater using L-arginine-functionalized Fe_3O_4 nanoparticles: Optimization, reusability, kinetic and equilibrium studies. J Magn Magn Mater 404:179–189
38. Karthikeyan P, Meenakshi S (2021) Fabrication of hybrid chitosan encapsulated magnetic-kaolin beads for adsorption of phosphate and nitrate ions from aqueous solutions. Int J Biol Macromol 168:750–759
39. Chen L, Wu P, Chen M, Lai X, Ahmed Z, Zhu N, Liu T (2018) Preparation and characterization of the eco-friendly chitosan/vermiculite biocomposite with excellent removal capacity for cadmium and lead. Appli Clay Sci 159:74–82
40. Son EB, Poo KM, Mohamed HO, Choi YJ, Cho WC, Chae KJ (2018) A novel approach to developing a reusable marine macroalgae adsorbent with chitosan and ferric oxide for simultaneous efficient heavy metal removal and easy magnetic separation. Bioresour Technol 259:381–387
41. Pereira FA, Sousa KS, Cavalcanti GR, França DB, Queiroga LN, Santos IM, Jaber M (2017) Green biosorbents based on chitosan-montmorillonite beads for anionic dye removal. J Environ Chem Eng 5(4):3309–3318

42. Chen YW, Lee HV, Juan JC, Phang SM (2016) Production of new cellulose nanomaterial from red algae marine biomass Gelidium elegans. Carbohydr Polym 151:1210–1219
43. Şenol ZM (2021) A chitosan-based composite for absorption of uranyl ions; mechanism, isothems, kinetics and thermodynamics. Int J Biol Macromol 183:1640–1648
44. Hu Y, Zheng X, Liu S, Peng X, Dai H, Hu F, Xu G (2021) Prediction and optimization of adsorption performance of MC@ MgAl-LDH for the removal of humic acid from aqueous solution: BBD model and mechanism. J Solid State Chem 302:122377
45.] E. Natarajan, G.P. Ponnaiah, Optimization of process parameters for the decolorization of Reactive Blue 235 dye by barium alginate immobilized iron nanoparticles synthesized from aluminum industry waste, Environ. Nanotechnol. Monit. Manage. 7 (2017) 73–88.
46. Lagergren S (1898) Zur theorie der sogenannten adsorption geloster stoffe. Vet Akad Handl 24:1–39
47. Ho YS, McKay G (1998) Sorption of dye from aqueous solution by peat. Chem Eng J 70:115–124
48. Subhan H, Alam S, Shah LA, Khattak NS, Zekker I (2022) Sodium alginate grafted hydrogel for adsorption of methylene green and use of the waste as an adsorbent for the separation of emulsified oil. J Water Process Eng 46:102546
49. Langmuir I (1918) The adsorption of gases on plane surfaces of glass, mica and platinum. J Am Chem Soc 40:1361–1403
50. Frenudlich HMF (1906) Over the adsorption in solution. J Phys Chem 57:385–471
51. Temkin MI (1940) Kinetics of ammonia synthesis on promoted iron catalysts. Acta physiochim URSS 12:327–356
52. Saleh TA, Elsharif AM, Bin-Dahman OA (2021) Synthesis of amine functionalization carbon nanotube-low symmetry porphyrin derivatives conjugates toward dye and metal ions removal. J Mol Liq 340:117024
53. Hoseinzadeh H, Hayati B, Ghaheh FS, Seifpanahi-Shabani K, Mahmoodi NM (2021) Development of room temperature synthesized and functionalized metal-organic framework/graphene oxide composite and pollutant adsorption ability. Mater Res Bullet 142:111408
54. Sarojini G, Babu SV, Rajamohan N, Rajasimman M (2022) Performance evaluation of polymer-marine biomass based bionanocomposite for the adsorptive removal of malachite green from synthetic wastewater. Environ Res 204:112132
55. Liu H, Chen L, Ding J (2016) Adsorption behavior of magnetic amino-functionalized metal–organic framework for cationic and anionic dyes from aqueous solution. RSC Adv 6:48884–48895
56. Sadiq AC, Olasupo A, Rahim NY, Ngah WSW, Suah FBM (2021) Comparative removal of malachite green dye from aqueous solution using deep eutectic solvents modified magnetic chitosan nanoparticles and modified protonated chitosan beads. J Environ Chem Eng 9(5):106281
57. Nethaji S, Sivasamy A, Thennarasu G, Saravanan S (2010) Adsorption of Malachite Green dye onto activated carbon derived from Borassus aethiopum flower biomass. J Hazard Mater 181(1–3):271–280
58. Mirmohseni A, Dorraji MS, Figoli A, Tasselli F (2012) Chitosan hollow fibers as effective biosorbent toward dye: preparation and modeling. Bioresour Technol 121:212–220
59. Reghioua A, Barkat D, Jawad AH, Abdulhameed AS, Khan MR (2021) Synthesis of Schiff's base magnetic crosslinked chitosan-glyoxal/ZnO/Fe_3O_4 nanoparticles for enhanced adsorption of organic dye: Modeling and mechanism study. Sustain Chem Pharm 20:100379
60. Phan DN, Rebia RA, Saito Y, Kharaghani D, Khatri M, Tanaka T, Kim IS (2020) Zinc oxide nanoparticles attached to polyacrylonitrile nanofibers with hinokitiol as gluing agent for synergistic antibacterial activities and effective dye removal. J Ind Eng Chem 85:258–268
61. Auta M, Hameed BH (2014) Optimized and functionalized paper sludge activated with potassium fluoride for single and binary adsorption of reactive dyes. J Ind Eng Chem 20(3):830–840
62. Jawad AH, Abdulhameed AS, Hanafiah MAKM, ALOthman, Z. A., Khan, M. R., & Surip, S. N. (2021) Numerical desirability function for adsorption of methylene blue dye by sulfonated pomegranate peel biochar: Modeling, kinetic, isotherm, thermodynamic, and mechanism study. Korean J Chem Eng 38(7):1499–1509
63. Hızal J, Kanmaz N, Yılmazoğlu M (2021) Adsorption efficiency of sulfonated poly (ether ether ketone)(sPEEK) as a novel low-cost polymeric adsorbent for cationic organic dyes removal from aqueous solution. J Mol Liq 322:114761
64. Singh SK, Das A (2015) The n → π* interaction: a rapidly emerging non-covalent interaction. Phys Chem Chem Phys 17(15):9596–9612